Biosensors and Bioelectronics 306 (2026) 118720

Contents lists available at ScienceDirect

Biosensors and Bioelectronics

journal homepage: www.elsevier.com/locate/bios

Real-time, label-free impedimetric monitoring of insulin secretion from three-dimensional stem cell–derived islets

Franziska Dana Zitzmann [a,b,1], Caroline Remmert [c,1], Nicole Katarina Rogers [d], Sabine Schmidt [a], Heiko Lickert [d,e], Heinz-Georg Jahnke [a,*], Matthias Meier [a,c,**]

[a] Center of Biotechnology and Biomedicine, University of Leipzig, Leipzig, Germany
[b] b-ACT matter, Research and Transfer Centre for bioactive Matter, Leipzig University, Leipzig, Germany
[c] Helmholtz Pioneer Campus, Helmholtz Zentrum München, Munich, Germany
[d] Institute of Diabetes and Regeneration Research, Helmholtz Zentrum München, Munich, Germany
[e] German Center for Diabetes Research (DZD), Neuherberg, Germany

ARTICLE INFO

Keywords:
hiPSC derived islets and β-cells
Electrochemical impedance spectroscopy
Microcavity arrays
Spatial resolved monitoring
Label-free secretion profiling
Glucose stimulated insulin secretion GSIS

ABSTRACT

Functional assessment of insulin secretion is essential for the development and application of stem cell–derived β-cell products. Conventional glucose-stimulated insulin secretion (GSIS) assays rely on end-point, batch-averaged enzyme-linked immunosorbent assays (ELISA), limiting temporal resolution and masking functional heterogeneity at the level of individual islet-like clusters. Here, we present a label-free, non-invasive impedance spectroscopy–based approach for real-time monitoring of insulin secretion from individual stem cell–derived islets (SC-islets) cultured on microcavity microelectrode array (MEA) chips. Human induced pluripotent stem cells were differentiated into SC-islets and integrated into microcavity MEAs, enabling three-dimensional confinement and parallel electrical recordings. Impedance measurements during on-chip GSIS revealed characteristic glucose-responsive dynamics that correlated with insulin secretion quantified by ELISA and were suppressed by pharmacological inhibition. Impedance spectroscopy resolved functional responses at the level of individual SC-islets, uncovering cluster-to-cluster variability that was obscured by pooled secretion assays. High-density microcavity MEAs further enabled spatially resolved impedance measurements, revealing intra-cluster heterogeneity of insulin secretion. While impedance spectroscopy provides an indirect readout and glucose stimulation was applied as stepwise changes, this platform enables real-time, scalable, and cluster-resolved functional assessment of three-dimensional islet tissues. The approach establishes a foundation for functional screening of SC-islets, differentiation optimization, drug testing, and future potency assessment workflows.

1. Introduction

Diabetes mellitus is a chronic metabolic disorder characterized by insufficient insulin secretion and/or impaired insulin action and is mainly classified into type 1 and type 2 diabetes (T1DM and T2DM). Worldwide, more than 583 million people are affected by diabetes, with incidence rates continuing to rise (Genitsaridi et al., 2025). The pathogenesis of diabetes ultimately involves the destruction or dysfunction of insulin-producing pancreatic β-cells. In T1DM, autoimmune-mediated β-cell destruction results in insulin deficiency and chronic hyperglycemia (Henriques et al., 2025). While current first-line therapies effectively manage blood glucose levels and insulin resistance, they do not restore lost β-cell mass or function (Faradji et al., 2019). Consequently, cell replacement therapies have emerged as a promising strategy to re-establish endogenous insulin secretion, improve glycemic control, reduce hypoglycemic episodes, and prevent long-term diabetes-associated complications (Latres et al., 2019; Shapiro et al., 2017). However, the widespread clinical application of pancreatic or islet transplantation remains limited by donor organ scarcity and the requirement for lifelong immunosuppression (Marfil-Garza et al., 2022; Yue et al., 2024).

Human induced pluripotent stem cells (hiPSCs) offer an attractive

* Corresponding author.
** Corresponding author. Center of Biotechnology and Biomedicine, University of Leipzig, Leipzig, Germany.
E-mail addresses: heinz-georg.jahnke@bbz.uni-leipzig.de (H.-G. Jahnke), matthias.meier@uni-leipzig.de (M. Meier).
[1] Authors contributed equally.

https://doi.org/10.1016/j.bios.2026.118720
Received 2 February 2026; Received in revised form 1 April 2026; Accepted 20 April 2026
Available online 24 April 2026

alternative source of insulin-producing cells, as they can be differentiated into β-like cells (SC-β-cells) through multi-stage protocols that recapitulate pancreatic development (Hogrebe et al., 2020; Pagliuca et al., 2014; Velazco-Cruz et al., 2019). These stem cell-derived islets (SC-islets) have broad applications in diabetes research, including cell replacement therapy (Carlsson et al., 2025; Siehler et al., 2021b; Wang et al., 2024), modeling islet development and function, studying diabetes pathogenesis (Balboa et al., 2021; Rosado-Olivieri et al., 2019; Russell et al., 2020), and screening for anti-diabetic drugs (Amin et al., 2018; Hu et al., 2025; Szabat et al., 2015). Despite substantial progress, current differentiation protocols yield SC-islets with considerable heterogeneity and a large fraction of functionally immature cells (Cuesta-Gomez et al., 2022; Veres et al., 2019a). Improving the reproducibility, maturation, and functional competence of SC-islets and β-cells therefore remains a major challenge (Lithovius et al., 2024; Mahaddalkar et al., 2020; Siehler et al., 2021c).

Functional β-cells are defined by their ability to secrete insulin in response to elevated glucose levels. Accordingly, glucose-stimulated insulin secretion (GSIS) assays followed by enzyme-linked immunosorbent assay (ELISA)-based insulin quantification represent the current gold standard for assessing β-cell function (Glieberman et al., 2021). While highly sensitive and specific, ELISA-based GSIS assays are labor-intensive, costly, and restricted to end-point measurements, limiting temporal resolution and masking functional heterogeneity at the level of individual islet-like clusters (MacDonald and Gapinski, 1989; Molano et al., 2024). These limitations hinder high-throughput screening of SC-islets and restrict their use for large-scale differentiation optimization and drug discovery.

Previous studies on bioelectronic monitoring of pancreatic islets and β-cell functionality have shown that glucose stimulation induces characteristic electrophysiological changes, including oscillatory membrane depolarization and synchronized bursting behavior, correlating with intracellular calcium dynamics and pulsatile insulin secretion (Alassaf et al., 2020; Schönecker et al., 2014). Accordingly, labor-intensive patch-clamp techniques have been used to analyze electrophysiological activity, alongside planar microelectrode arrays (MEAs) for field potential monitoring (Jaffredo et al., 2023). However, MEA-based studies to date primarily rely on dispersed cells or planar configurations and lack volumetric confinement, limiting their ability to capture functional responses within a controlled three-dimensional microenvironment.

Although this has not yet been directly demonstrated, we hypothesized that β-cell activation leading to insulin secretion and thus β-cell functionality should be detectable via impedance spectroscopy. From a physiological perspective, insulin secretion by β-cells is tightly coupled to glucose-induced membrane depolarization, calcium influx through voltage-gated calcium channels, and subsequent exocytosis of insulin granules (Campbell and Newgard, 2021). These processes are accompanied by dynamic changes in membrane capacitance and resistance, suggesting that insulin secretion events can be indirectly monitored through impedance-based electrical readouts.

In contrast to planar, surface-limited electrophysiological measurements obtained by field potential monitoring (Kim et al., 2025; Yang et al., 2024), impedance spectroscopy, particularly when combined with microcavity array (MCA) platforms, has been successfully applied to the analysis of three-dimensional cell cultures. This includes the assessment of cytotoxicity, barrier function(Mathew-Schmitt et al., 2025), drug penetration(Poenick et al., 2014), as well as cell morphology and contractility(Fleischer et al., 2019; Zitzmann et al., 2024). Moreover, high-resolution impedance spectra enable inference of structural and functional properties within three-dimensional cultures and organoids (Jahnke et al., 2014; Zitzmann et al., 2022).

In this study, we present an impedance spectroscopy-based approach for monitoring insulin secretion from individual SC-islets using MCA chips. By performing GSIS directly on-chip, we demonstrate that impedance changes reliably reflect glucose-induced insulin secretion dynamics. Furthermore, pharmacological inhibition of calcium influx using diazoxide results in a corresponding suppression of impedance responses, confirming the functional specificity of the electrical signal. Additionally, we demonstrate, the use of multi-impedance spectra analysis to achieve spatial resolution for β-cell functionality within single SC-islets. Together, our results establish impedance spectroscopy as a fast, non-invasive, and scalable method for functional screening of SC-islets, with potential applications in SC-β-cell maturation assessment, differentiation protocol optimization, and high-throughput anti-diabetic drug screening.

2. Material and methods

2.1. Fabrication of microcavity arrays

Fused silica microcavity arrays (MCAs) were fabricated using a two-step process comprising (i) glass structuring by selective laser-induced etching (SLE) and (ii) microelectrode patterning via a lift-off process, as previously described (Zitzmann et al., 2022). Two MCA designs were used in this study. The first design featured 14 microcavities with square base areas and lateral dimensions ranging from 150 to 450 μm, all sharing a common medium reservoir. The second design consisted of octagonally shaped microcavities with a uniform diameter of 300 μm, each integrated into an individual medium reservoir. Cavity layouts were designed using CAD software (Autodesk Inventor Professional; USA) and modeled as inverted frustums of pyramids, with heights corresponding to two-thirds of the base side length. The designs were converted into machine code using CAM software (Alphacam, Vero Software GmbH, Germany). Glass substrates (4-inch quartz wafers, MicroChemicals GmbH, Germany) were processed using a selective laser etching system (FEMTOprint f200aHead 2 PP, Switzerland) mounted on an XY linear translation stage. Structures were inscribed using a 1030 nm Yb:YAG laser (pulse energy: 230 nJ; pulse duration: 400 fs) in multiple passes. Subsequently, the laser-processed substrates were etched in 45 wt% KOH solution at 84 °C using a pulsed ultrasonic bath. The structured glass base measured 49 mm × 49 mm, with microcavities located centrally. Each cavity wall contained an integrated microelectrode with a surface area of approximately 0.11 mm^2, depending on cavity size. Electrical connections were established via conductive paths (0.05 mm width) extending from each electrode to the edge of the glass substrate, where they terminated in enlarged contact pads (0.5–0.7 mm). Microelectrodes were fabricated using a lift-off process, as previously described (Zitzmann et al., 2022).

2.2. Human induced pluripotent stem cell culture

hiPSCs were cultured on tissue culture plates coated with diluted Geltrex (Life Technologies, Cat#A1413302) in StemMACS™ iPS-Brew medium (Miltenyi Biotec, Cat#130104368). Cells were maintained under standard culture conditions (37 °C, 5 % CO_2), and the medium was changed daily. hiPSCs were passaged at approximately 70 % confluency using 0.5 mM EDTA (AppliChem, Cat#A4892). Mycoplasma testing was performed routinely using the MycoAlert PLUS Mycoplasma Detection Kit (Lonza, Cat#LT07-703) according to the manufacturer's instructions. The hiPSC line HMGUi001-A or the C-peptide–mCherry reporter clone HMGUi001-A-820 was used in this study.

2.3. Differentiation of stem cell–derived β-cells and generation of stem cell–derived islets

hiPSCs were differentiated into SC-islets according to a previously published protocol (Velazco-Cruz et al., 2019). Briefly, hiPSCs were dissociated into single cells and seeded at a density of 0.6 × 10^6 cells mL^{-1} in either 30 mL spinner flasks or 6-well ultra-low attachment (ULA) plates (Corning, Cat#3471) in the presence of 10 μM ROCK inhibitor Y-27632 (Biozol, Cat#APE-A3008-10). Prior to differentiation,

cells were cultured as three-dimensional aggregates for at least 2 days. Differentiation was performed using a six-stage protocol to generate SC-β-cells. At the beginning of stage 6 (S6), aggregates were re-dispersed to reduce off-target cell populations. For this purpose, cells were washed with PBS, dissociated using Accutase (Sigma-Aldrich, Cat#A6964) for approximately 30 min, and filtered through a 40 μm cell strainer (pluriSelect, Cat#43-10040-40). Single cells were reseeded at a density of 1×10^6 cells mL^{-1} in ULA plates in S6 medium supplemented with 10 μM ROCK inhibitor and cultured on an orbital shaker at 100 rpm under standard culture conditions. Medium was changed daily during the first 14 days of S6 and every other day thereafter. Differentiated SC-islets were identified by mCherry fluorescence, indicating insulin-positive SC-β-cells. The composition of the S6 medium is provided in Table 1.

2.4. Flow cytometry

SC-islets were dissociated using 5 ml TrypLE™ Select (1x, Thermo Fisher Scientific, Gibco 12563011) for 8-12 min at 37 °C. Dissociation reagent was stopped using 10 ml hiPSC Brew or S6 base media, respectively. Cells were centrifuged for 3 min and fixed with 4 % PFA for 10 min at room temperature, washed with −/− DPBS, and stored at 4 °C or used for flow cytometric analysis. For immunostaining, cells were placed in a 96 well plate (Thermo Fischer Scientifiv, 277143), permeabilized with permeabilization buffer consisting of Milli Q water with 0.1 M Glycine (Merck, Sigma Aldrich G8898-1 KG) and 0.2 % Triton-x 100 (Merck, Sigma Aldrich, T8787-250 ML). Cells were blocked with blocking solution (10% FBS (PAN Biotech, P40-37500), 0.1% BSA (Merck, Sigma-Aldrich A3311-100G), 3% donkey serum (Merck, Millipore S30-100 ml), 0.1% Tween-20 (Merck, Sigma-Aldrich, P2287-500 ML) in 1x PBS) for 30 min at room temperature. Antibodies were diluted in blocking serum and incubated for 1 h at room temperature. Cells were washed with −/−DPBS, strained using 5 mL Polystyrene Round Bottom Tube with Cell-Strainer (Corning, Falcon 3522235) and analyzed using BD FACSAria III and processed using Flowjo (Version 10.07.2001, Becton Dickinson).

2.5. Impedance spectroscopy monitoring of SC-islets

For impedance measurements, SC-islets were manually selected based on size and mCherry fluorescence and starved for 2 h in Krebs–Ringer buffer (KRB) containing 2.8 mM glucose (129 mM NaCl, 4.8 mM KCl, 1.2 mM KH_2PO_4, 1.2 mM $MgSO_4$, 2 mM $CaCl_2$, 24 mM $NaHCO_3$). Aggregates were subsequently transferred into the microcavities of the MCA chips. After 1h resting time impedance spectra were recorded using a precision impedance analyzer (Agilent 4294A) controlled by custom-developed software (IMATadvanced v2.2.5.3). Measurements were performed over a frequency range from 500 Hz to 5 MHz with 51 logarithmically spaced frequency points, applying a ±10 mV AC excitation at 0 V bias. Baseline impedance was recorded for 10 min under low-glucose conditions (2.8 mM), followed by stimulation with 20 mM glucose and continuous recording for 40 min. Subsequently, KCl was added to a final concentration of 30 mM, and impedance was recorded for additional 30 min. For secreted insulin quantification, 150 μL of buffer was collected from a total reservoir volume of 1.5 mL and replaced by 150 μL of a 10x concentrated glucose (200 mM) or KCl (300 mM) stock. Rapid mixing was ensured by gentle pipetting several times. For single SC-islet analysis the total reservoir volume was 200 μL and the collected sample volume as well as the replacement volume was 30 μL due to limit of detection issues of the ultra-sensitive insulin ELISA kit (Mercodia, Cat#10113201). Temporary interruptions in impedance recording (up to 3 min) occurred during buffer exchange due to incubator access. For inhibition experiments, 250 μM diazoxide (Sigma, Cat#D9035) was included in the low glucose buffer. For taking changes of buffer conductivity, especially for KCl application, into account blank values without SC-islets were recorded for each experiment. The solvent resistance was determined by equivalent circuit fitting and all experiment impedance spectra were corrected for the appropriate buffer situation. Relative impedance as a representation for the cell/cluster signal was calculated as $(|Z|_{(\text{cell covered})} - |Z|_{(\text{cell-free})})/|Z|_{(\text{cell-free})} \times 100$ % using custom analysis software (IDAT v3.6.5.2). The frequency at which the relative impedance reached its maximum was identified and tracked over time. Where indicated, impedance traces were normalized to the start of the experiment.

Table 1
S6 medium.

REAGENTS	FINAL CONCENTRATION	VOLUME for 100 ml [ml]
MCDB131 medium		100
Glucose	0.46 g l^{-1}	0.23
BSA	0.02 g ml^{-1}	2.1 g
GlutaMAX 100x	1x	1.04
P/S 100x	1x	1.04
MEM non-essential amino acids 100x	1x	1.04
Trace elements A 1000x	1x	0.105
Trace elements B 1000x	1x	0.105
ZnSO4 10 mM	10 μM	0.105
Heparin 50 mg/ml	10 μg ml^{-1}	0.02

2.6. ELISA-based detection of insulin secretion

ELISA samples were collected after each stimulation step of the GSIS experiments and analyzed for insulin content by ELISA. The assay was performed according to the manufacturer's instructions (Ultrasensitive Insulin ELISA, Mercodia, 10-1132-01) using a 25 μL sample volume. Temporary interruptions in impedance recording (up to 3 min) occurred during buffer exchange due to incubator access.

2.7. Microscopy and immunofluorescence

For immunofluorescence staining, samples were fixed in 4 % paraformaldehyde for 30 min at room temperature washed with −/− DPBS, and cryoprotected using a sucrose gradient (10 % and 30 % w/v, 2 h each at room temperature). Samples were then incubated overnight at 4 °C in a 1:1 mixture of 30 % sucrose and tissue freezing medium (Leica, Cat#14020108926), embedded in cryomolds, and frozen on dry ice. Cryosections (10 μm thickness) were prepared using a cryostat. Sections were air-dried for 30 min, rehydrated in −/− DPBS for 20 min, and permeabilized for 20 min in −/− DPBS containing 0.1 M glycine and 0.1 % Triton X-100. Blocking was performed for 2 h at room temperature in blocking buffer (10 % fetal calf serum, 0.1 % BSA, 3 % donkey serum, 0.1 M glycine in DPBS with 0.2 % Tween-20). Primary antibodies were applied overnight at 4 °C: guinea pig anti-insulin (1:300, Bio-Rad, Cat#53300104G), mouse anti-glucagon (1:2000, Sigma, Cat#G2654), and rabbit anti-NKX6.1 (1:100, Cell Signaling Technology, Cat#54551S). After washing, sections were incubated with secondary antibodies (1:500) for 3 h at RT: anti-guinea pig Cy3, anti-mouse Alexa Fluor 647, and anti-rabbit Alexa Fluor 488. Sections were mounted using Vectashield mounting medium (Vector Laboratories, Cat#VEC-H-1900-10) and imaged using a Zeiss LSM 880 confocal microscope.

2.8. Statistics

Graphpad Prism 9 (GraphPad Software, USA) was used for displaying data in graphs and all statistical analysis. To test for significant effects, normal distribution was ensured by Shapiro-Wilk test and two-group comparison was performed by Welch's *t*-test. Effects were considered as significant with * = $p < 0.05$, ** = $p < 0.01$, *** = $p < 0.001$.

3. Results and discussion

3.1. Characterization of stem cell–derived islets for impedance spectroscopy

For impedimetric analyses, hiPSCs were differentiated into SC-islets using a six-stage protocol following pancreatic development (Velazco-Cruz et al., 2019). As reported for this and other stem cell–based islet differentiation protocols, SC-islets comprise heterogeneous cell populations encompassing multiple endocrine lineages and a range of functional maturation states (Veres et al., 2019a). Endocrine differentiation was assessed by marker-based analyses. Immunostaining confirmed the presence of insulin- and NKX6.1–positive SC-β-cells and glucagon-positive stem cell–derived α-cells (SC-α-cells) within SC-islets (Fig. 1A).

To quantitatively assess endocrine cell composition, flow cytometry analysis was performed at the early stage 6 (S6) time point (day 21 of differentiation). At this stage, 26 % of cells were insulin-positive, whereas glucagon-positive cells were not detected (Fig. 1B). At day 21, SC-islets were subjected to one of two maturation strategies: clusters were either maintained intact and matured for an additional 14 days, or enzymatically dissociated into single cells and reaggregated prior to an additional 14 days of maturation. This reaggregation strategy was implemented based on previous reports demonstrating that controlled reaggregation and resizing of stem cell–derived endocrine cells can support functional maturation by promoting defined cluster architecture and cell–cell interactions (Velazco-Cruz et al., 2019; Veres et al., 2019a).

At the end of stage 6 (day 35), endocrine composition was reassessed by flow cytometry. Analyses were performed across six independent differentiation experiments, of which a representative example is shown. Both SC-islets and reaggregated SC-islets exhibited comparable endocrine cell fractions, with insulin-positive β-cells accounting for 20 % ± 6 % and glucagon-positive α-cells accounting for 17 % ± 8 % in each condition. All experiments were performed using the same parental hiPSC line. In two of the six experiments, an isogenic mCherry–insulin reporter hiPSC line was used (Siehler et al., 2021a), in which mCherry was introduced by CRISPR/Cas9-mediated knock-in into the endogenous INS locus in a heterozygous configuration, enabling direct visualization of insulin-expressing cells. Together, these results establish SC-islets as a reproducible 3D endocrine model suitable for investigating impedance spectroscopy functional analysis.

For initial impedimetric characterization, SC-islets were transferred into the MCA chips comprising fourteen microcavities, each equipped with four integrated gold microelectrodes and connected to a common medium reservoir (Fig. 1C). The chip's transparent glass substrate enabled brightfield and fluorescence microscopy to confirm the placement of individual SC-islets within the microcavities and to validate insulin expression using an isogenic mCherry–insulin reporter line (Fig. 1C, insets). After confirming correct SC-islet placement, impedance spectra were recorded over a frequency range of 5 kHz to 5 MHz for SC-islets (n = 7) and reaggregated SC-islets (n = 12), and relative impedance values were calculated as an expression of the cell/cluster signal (Fig. 1D). In both conditions, the spectra showed the characteristic frequency dependence of compact, spheroidal 3D cultures, a pronounced increase in relative impedance at low-to-intermediate frequencies, reaching a maximum signal amplitude at ~100–300 kHz, followed by a gradual decrease toward a plateau in the MHz range. Unlike the bell-shaped curve typically observed in 2D cultures, the MHz plateau reflects the cells' parallel resistance–capacitance behavior (Gerasimenko et al., 2020; Jahnke et al., 2014; Zitzmann et al., 2022) and likely arises from an additional series resistance imposed by the 3D culture architecture, as reported previously.

Comparison of the maximum relative impedance values revealed no significant difference between SC-islets and reaggregated SC-islets (Fig. 1E), indicating comparable bulk impedimetric signals at this differentiation stage. This observation is consistent with flow cytometry–based quality-control analyses, which showed similar overall fractions of insulin-positive cells in both conditions at the population level. In contrast, individual SC-islets exhibited substantial heterogeneity in impedance signal, as well as in composition, including the fraction of insulin-positive cells and their spatial distribution within the clusters (Fig. 1E and F). These findings highlight the need for a non-invasive approach to monitor functionality at the level of individual clusters.

3.2. Monitoring glucose-stimulated insulin secretion by impedance spectroscopy

To assess glucose-stimulated insulin secretion (GSIS), we established an on-chip impedance spectroscopy assay (Fig. 2A). SC-islets were sequentially exposed to low glucose (2.8 mM), high glucose (20 mM), and KCl-induced depolarization (30 mM) to trigger maximal insulin release, while impedance spectra were recorded every minute. Based on the equivalent circuit model (Fig. 2B) and the frequency dependence observed in Fig. 1D, analyses focused on the cellular parallel resistance–capacitance element, quantified as the maximum relative impedance amplitude in the 100–300 kHz range.

Time traces of the maximum relative impedance values revealed a characteristic response to glucose stimulation, consisting of an initial decrease in maximum relative impedance followed by a gradual recovery toward baseline levels (Fig. 2C). This response was consistently observed across individual SC-islets, although the magnitude of the impedance change varied in the range of 5-25 % between clusters, reflecting cluster-to-cluster variability in functional responses. The timing of the impedance response is consistent with known GSIS dynamics in primary human islets and stem cell–derived β-cell clusters, which exhibit a rapid triggering phase followed by sustained secretion (Henquin et al., 2006; Seino et al., 2011). While the impedance-based readout does not resolve discrete first- and second-phase insulin secretion, the temporal progression of the signal aligns with the physiological time window of insulin release. Notably, even in SC-islet systems reported in the literature, the second phase is not distinctly separated from the first but rather appears as a prolonged secretory phase (Siehler et al., 2024; Velazco-Cruz et al., 2019). Application of 30 mM KCl induced a rapid decrease in relative impedance to ~0–30% within 3 min, followed by a gradual recovery to ~60–80% over the subsequent 30 min. In contrast to non-reaggregated SC-islets, impedance responses of reaggregated SC-islets to 20 mM glucose exhibited reduced variability between clusters, resulting in a more homogeneous response pattern (max. relative impedance decrease of 17-25 %) under identical stimulation conditions. This observation is consistent with previous GSIS reports demonstrating that dissociation and controlled reaggregation can reduce functional variability by promoting more uniform cluster architecture and are accompanied by a loss of undifferentiated enterochromaffin-like cell populations (Velazco-Cruz et al., 2019; Veres et al., 2019b). Additionally, the application of 30 mM KCl to reaggregated SC-islets also revealed reduced variability between clusters. Together, these observations support the notion that reaggregation enhances functional maturity by reducing non-endocrine or off-target cell types that may interfere with glucose-responsive β-cell signaling.

To assess response specificity, undifferentiated hiPSC aggregates were analyzed as controls (Fig. 2E). Unlike SC-islets, these aggregates showed no glucose-dependent decrease in impedance, with maximum relative impedance remaining stable at ~100–105%. In contrast, stimulation with 30 mM KCl induced a rapid decrease to ~50–60%, albeit markedly attenuated compared with SC-islets. This response is consistent with the expression of functional potassium channels in hiPSCs, which can trigger membrane depolarization and cytosolic calcium influx and thereby elicit downstream cellular effects (Kaitsuka, 2024). While these results demonstrate β-cell specificity of the impedimetric signal, the precise cellular contributors cannot be fully disentangled. Upon glucose stimulation, ATP-dependent closure of K_ATP channels reduces

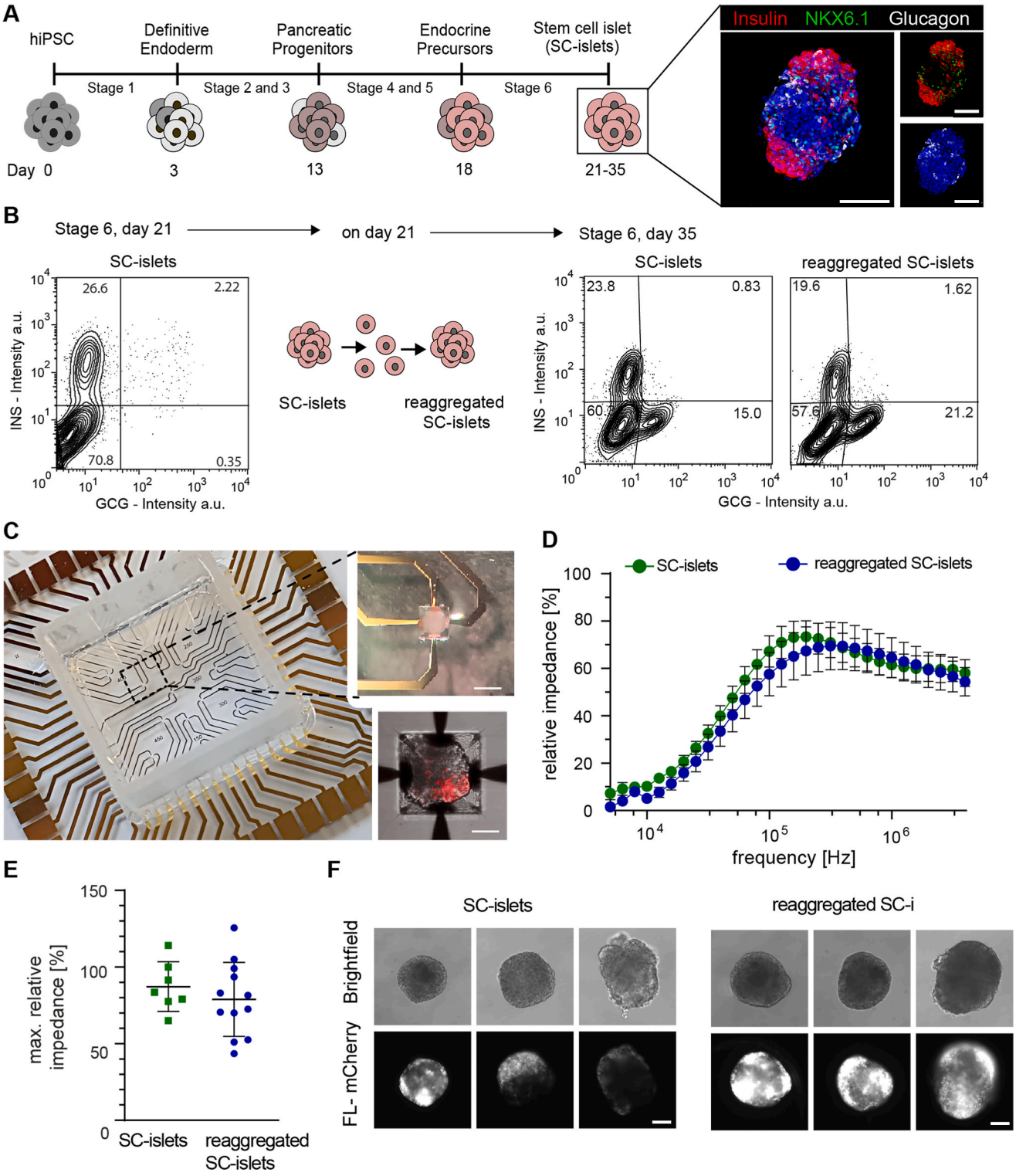

Fig. 1. Generation workflow and multimodal characterization of stem cell–derived islet (SC-islets) using impedance and fluorescence analyses. A) Differentiation scheme of SC-islets generated from human inducible pluripotent stem cells (hiPSCs). Shown is a representative immunofluorescence image of an SC-islet stained for insulin, glucagon, and NKX6.1 after 35 days of differentiation. Scale bars: 150 μm. **B)** Flow cytometric analysis of differentiation efficiency at day 21. At this stage, SC-islets are either further matured in culture or subjected to a disaggregation/reaggregation step to enhance insulin secretion. **C)** Microcavity array with 14 cavities containing four gold electrodes each integrated into a common medium reservoir. Insets show a brightfield image of a cavity containing a SC-islets (top) and a fluorescence/brightfield overlay of a single SC-islets derived from an hiPSC line carrying an mCherry–insulin reporter (bottom). Scale bars: 300 and 100 μm. **D)** Relative impedance spectra of SC-islets (green, $n_{cluster} = 7$) and reaggregated SC-islets (blue, $n_{cluster} = 12$) across the frequency range of 5000–5,000,000 Hz (mean ± SEM). **E)** Statistical analysis of the maximum relative impedance of SC-islets (green, $n_{cluster} = 7$) and reaggregated SC-islets (blue, n = 12) (mean ± SD). **F)** Representative brightfield (top) and fluorescence (bottom) images of mCherry–insulin–labeled SC-islets with and without reaggregation, differentiated to day 35. Scale bars: 100 μm. $n_{clsuter}$ represents the number of SC-islets per condition.

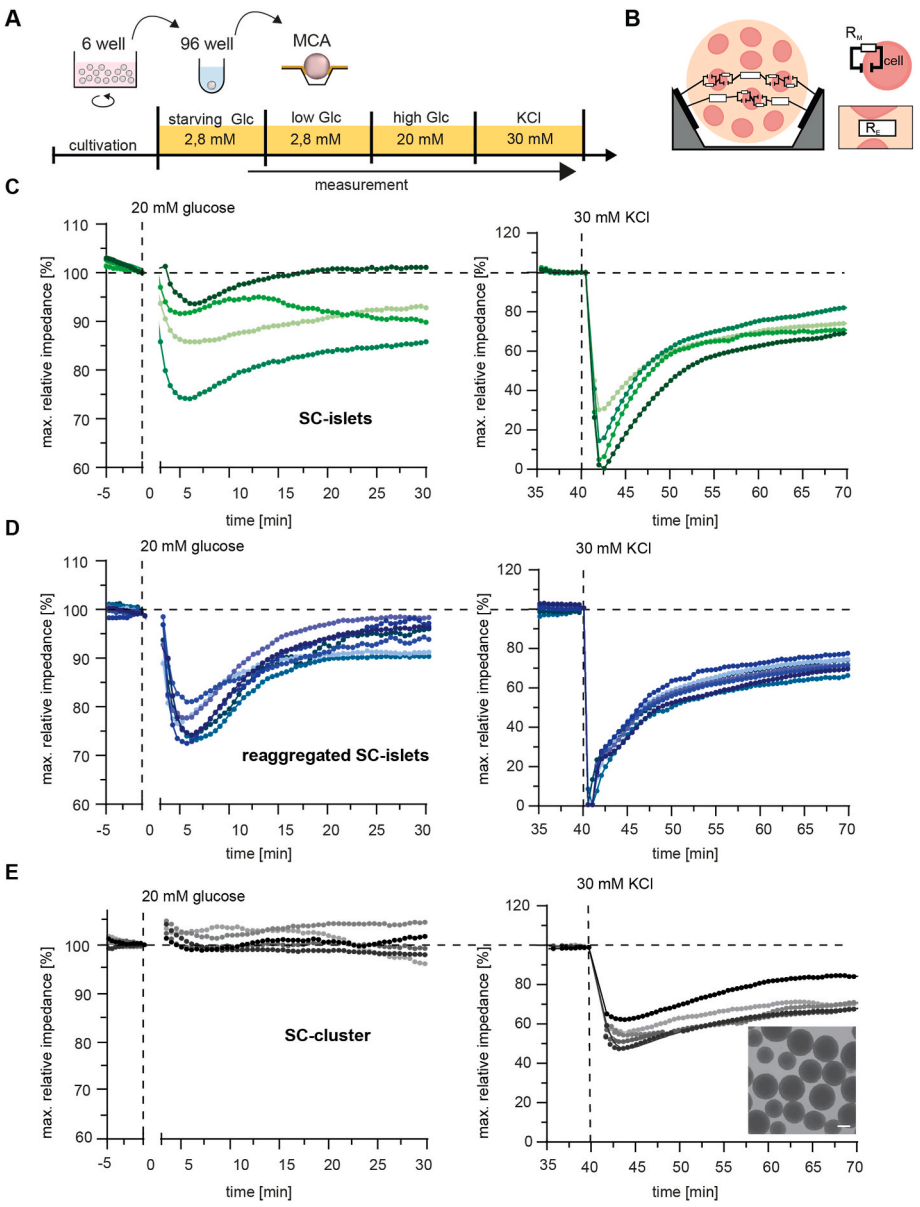

Fig. 2. Impedimetric analysis of glucose-stimulated insulin secretion (GSIS) in SC-islets. A) Schematic of the on-chip GSIS assay. **B)** Equivalent circuit diagram showing the expected resistive components on the microcavity MEA that influence the impedance signal: R_m = cell membrane resistance and R_e = extracellular space resistance. **C–E)** Time-resolved maximum relative impedance signals recorded from **C)** SC-islets (green, $n_{cluster}$ = 4 cluster), **D)** reaggregated SC-islets (blue, $n_{cluster}$ = 10 cluster), and **E)** non-differentiated hiPSC aggregates ($n_{cluster}$ = 5 cluster). All samples were exposed to a 20 mM high-glucose pulse followed by a 30 mM KCl depolarization pulse on chip. The dotted line indicates when the buffer was changed to the next higher concentration. The inset in (E) shows a brightfield image of undifferentiated hiPSC clusters used as a control culture. Scale bar: 100 μm. $n_{clsuter}$ represents the number of SC-islets per condition.

potassium conductance, leading to membrane depolarization and activation of voltage-gated Ca^{2+} channels. The resulting Ca^{2+} influx triggers insulin granule exocytosis (Meyer-Hermann, 2007). These processes are accompanied by dynamic changes in membrane resistance and capacitance arising from ion fluxes and vesicle fusion events, both of which contribute to the measured impedance response. In particular, increased ionic conductance during depolarization provides a plausible explanation for the observed transient decrease in impedance (Müller et al., 2023). Although individual electrophysiological events occur on a millisecond timescale and are not directly resolved by impedance spectroscopy, their integrated effect at higher activity levels is expected to manifest as an apparent reduction in membrane resistance over longer timescales. Additional contributions from exocytosis-related membrane remodeling cannot be excluded. Together with the correlation to ELISA-based insulin measurements and the suppression of the signal upon pharmacological inhibition of β-cell depolarization, these findings support that the impedance readout captures functionally relevant aspects of glucose-stimulated β-cell activity.

Although the cause for the impedimetric signal has not yet been fully resolved, the experimental results demonstrate that impedance spectroscopy enables real-time, single-cluster–resolved monitoring of GSIS in hiPSC derived islet-like clusters and reveals reaggregation-induced functional maturation that is not captured by β-cell fraction alone.

3.3. *Comparison of impedimetric monitoring with ELISA-based insulin quantification*

To correlate the impedance spectroscopy–based GSIS readout with insulin secretion, culture supernatants were collected from the shared MCA chip reservoir after each stimulation step and analyzed by ELISA.

Consistent with standardized batch quality-control protocols and the chip's common-reservoir design, these measurements report the cumulative insulin secretion of all SC-islets within a single MCA experiment.

Reproducibility was ensured by analyzing SC-islets derived from seven independent differentiation experiments, including both non-reaggregated and reaggregated clusters to account for inter-batch variability. Time-resolved analysis of the maximum relative impedance change during glucose stimulation revealed reproducible, glucose-dependent responses across all differentiation batches (Fig. 3A). According to the averaged maximum relative impedance trace for each experiment, the magnitude of the impedance response varied between 5 and 20 %, reflecting batch-to-batch differences in differentiation efficiency, the overall temporal profiles and characteristics of the impedance responses were highly consistent, indicating robust and reproducible impedance signatures of GSIS.

To test the pharmacological specificity of the impedance readout, SC-islets from three independent differentiation batches were treated in parallel with diazoxide, a selective potassium channel (Kir6.2) opener that suppresses β-cell insulin secretion and is clinically used to treat hyperinsulinemic hypoglycemia. Diazoxide was applied prior to glucose stimulation and mean maximum relative impedance traces from each experiment were averaged (Fig. 3B). Diazoxide-treated SC-islets showed a strongly attenuated impedance response compared with untreated controls, remaining close to baseline throughout stimulation. Statistical analysis of the maximal relative impedance decreases within the first 15 min after high-glucose exposure confirmed a highly significant inhibition (Fig. 3C). This response is consistent with inhibition of glucose-induced membrane depolarization and insulin secretion upon potassium channel (Kir6.2) opening, demonstrating that the impedance signal reflects electrically and functionally coupled β-cell activity rather than nonspecific glucose-induced effects.

For validation, insulin secretion into the medium was quantified by ELISA using samples from five differentiation batches, including the three diazoxide inhibition experiments (Fig. 3C). The relative insulin release factor increased significantly in untreated SC-islets, whereas diazoxide markedly blunted this response. Consistent with the impedance measurements, diazoxide treatment significantly reduced both the glucose-induced impedance decrease and the ELISA-derived insulin stimulation index compared with non-inhibited controls, confirming effective pharmacological suppression of GSIS across both readout modalities. Moreover, at the level of individual differentiation experiments a direct linear correlation was observed between the impedance signal and the corresponding amount of insulin secretion determined by ELISA (Fig. 3D), indicating that impedance spectroscopy reliably captures GSIS-associated functional output. Notably, impedance measurements resolve functional heterogeneity between differentiation batches as well as for each batch on an individual SC-islet, whereas ELISA measurements integrate secretion across multiple clusters within each MCA (typically 4–6 SC-islets). As a result, intra-chip single-cluster heterogeneity is averaged in the biochemical readout, whereas impedance spectroscopy preserves higher functional resolution. Together, these findings highlight impedance spectroscopy as a complementary approach that provides additional insight into GSIS variability beyond what is accessible through batch-averaged ELISA measurements.

3.4. *Spatially resolved impedance monitoring reveal intra-cluster heterogeneity of insulin secretion*

Beyond analyzing the heterogeneity of individual SC-islets within batches, there is considerable interest in being able to analyze intra-cluster heterogeneity. To investigate whether impedance spectroscopy can resolve spatial heterogeneity of GSIS within individual SC-islets, a microcavity array chip with enhanced spatial resolution was employed (Fig. 4A). The chip design comprised six independent wells with 200 µl medium reservoir, each containing a single microcavity equipped with eight gold microelectrodes, enabling the acquisition of 28 impedance spectra for each possible electrode combination from the same SC-islet that encodes spatial information as previously demonstrated (Zitzmann et al., 2022).

Therefore, individual SC-islets were positioned into the

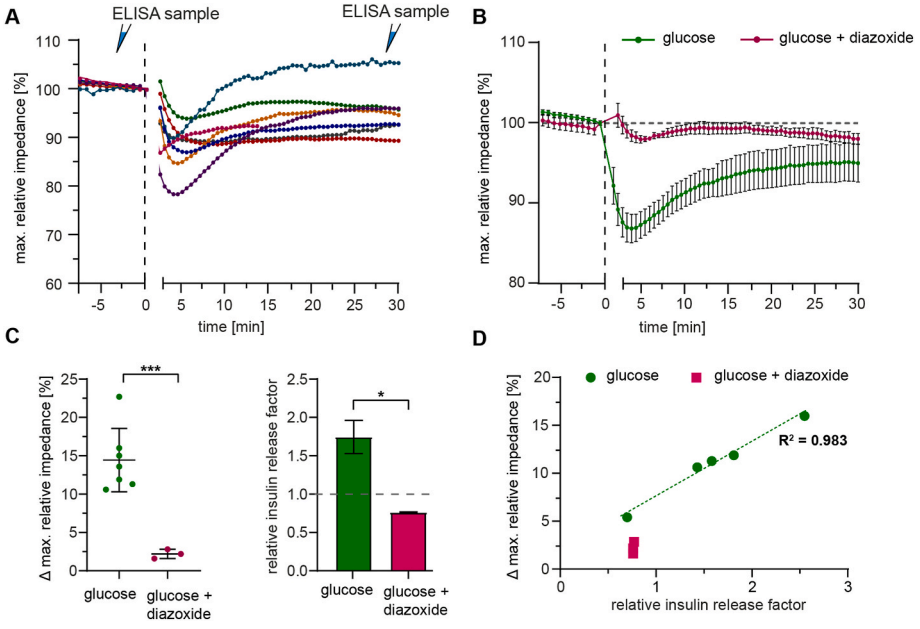

Fig. 3. Comparison of impedimetric insulin-release measurements after glucose stimulation with the gold-standard ELISA. A) Time-resolved analysis of maximum relative impedance changes during a GSIS from different differentiation batches of SC-islets ($n_{exp} = 9$, each with $n_{cluster} > 4$). **B**) Comparison of maximum relative impedance during the GSIS assay of SC-islets stimulated with glucose ($n_{exp} = 7$ experiments, each with $n_{cluster} > 4$) versus aggregates additionally treated with the inhibitor diazoxide ($n_{exp} = 3$ experiments, each with $n_{cluster} > 4$) (mean ± SEM). **C**) Statistical analysis of the maximum relative impedance decreases within the first 15 min after 20 mM glucose stimulation (left) and the corresponding insulin concentrations determined by ELISA are indicated by the stimulation index (right, glucose: $n_{exp}= 5$ experiments, gluc + diazoxide: $n_{exp}= 3$ experiments, * = $p < 0.05$, *** = $p < 0.001$.). **D**) Correlation analysis of measured insulin index with relative impedance showing a linear correlation for experimental derived mean values (from C).

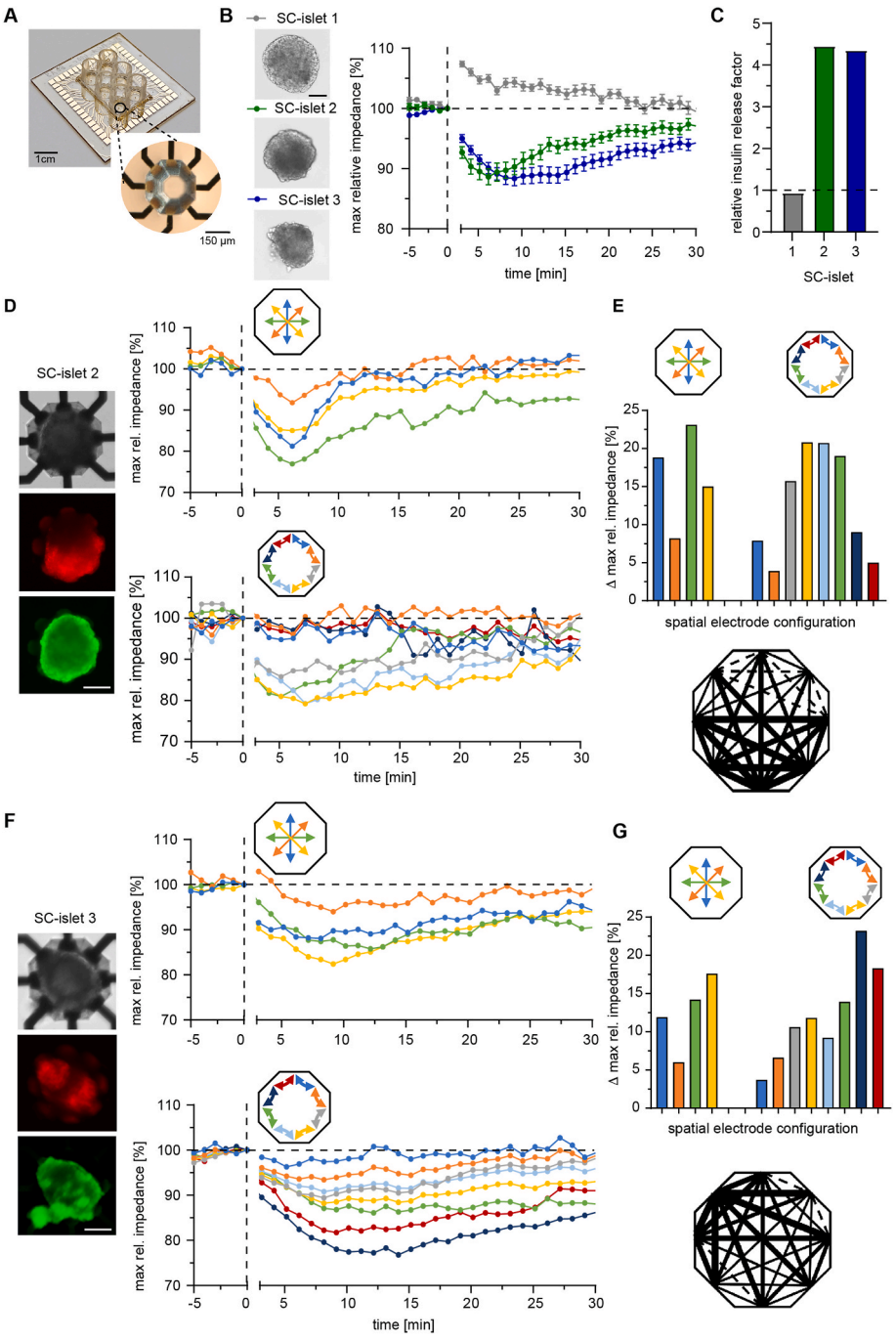

Fig. 4. Spatially resolved impedimetric analysis of glucose stimulated insulin secretion from individual SC-islets using microcavity MEA. A) Image of the chip platform with six wells, each containing a single microcavity. The magnified view shows the microcavity equipped with eight gold electrodes, providing increased spatial resolution of the impedance measurements. **B)** Brightfield images of the individual SC-islets used in the experiment. Scale bar: 100 µm. Also shown is the averaged time-resolved change in maximal relative impedance following glucose stimulation for SC-islet 1 (grey), SC-islet 2 (blue), and SC-islet 3 (green) corresponding to the clusters depicted in the images (mean ± SEM, $n_{electrode} = 28$ electrode combinations). In **C)**, the stimulation indices determined by ELISA for the three aggregates during the assay are presented. **D** and **F**) Individual impedimetric GSIS traces of SC-islet 2 and SC-islet 3 across different electrode pairs. To aid interpretation of spatial differences in the impedance profiles, fluorescence images of mCherry–insulin–labeled β cells within the corresponding SC-islets are provided. **E** and **G)** Maximum relative impedance decreases (Δ maximum relative impedance) across individual electrode pairs following the addition of 20 mM glucose in mCherry–insulin–labeled SC-islet 2 and SC-islet 3. The lower panels show the graph-weighted maximum relative impedance signals for all possible electrode pairs. $n_{electrode}$ represents the number of electrodes.

microcavities, and brightfield imaging was used to document cluster morphology prior glucose stimulation (Fig. 4B). Time-resolved impedance changes were recorded following glucose stimulation and maximum relative impedance values averaged for all 28 electrode combinations for each SC-islet. Representative SC-islets from one batch were selected for spatially resolved analysis. Whereas two SC-islets displayed glucose-responsive impedance dynamics with temporal profiles consistent with previous observations (see Fig. 3), one SC-islet lacked the characteristic response pattern (Fig. 4B). For validation, insulin secretion from each individual SC-islet was quantified by ELISA. Although single-cluster measurements were constrained by limited sample volume and the assay's detection limit, increasing the

withdrawal volume to 30% (65 μL) instead of 10% and using undiluted samples enabled determination of relative insulin release factors (Fig. 4C). These results corroborated the impedimetric readout, including for the non-responsive SC-islet 1.

To resolve spatial heterogeneity within the two responsive SC-islets, impedance traces were analyzed across all 28 electrode combinations and are shown exemplarily for transverse and laterally adjacent electrode pairs (Fig. 4D/F). Within each cluster, glucose stimulation induced qualitatively similar GSIS dynamics across electrode pairs, whereas the response amplitude varied depending on electrode position. For correlation, SC-islets were stained with calcein AM after the experiment to confirm viability and were imaged by fluorescence microscopy while maintaining their orientation within the microcavities. Fluorescence images of mCherry–insulin–labeled β-cells are shown alongside the impedance traces to provide cellular context. Quantification of the maximum impedance change for each electrode pair (Fig. 4E/G) revealed that electrode pairs spanning regions with stronger reporter signal exhibited larger impedance responses, whereas pairs traversing regions with weaker reporter signal showed attenuated responses. Although neither impedance spectroscopy nor microscopy provides z-axis resolution, these data demonstrate a clear qualitative correlation in the xy-plane, indicating that spatial impedance profiles reflect the distribution of insulin-expressing cells within individual SC-islets.

Thus, quantitative differences of the maximum relative impedance effect between electrode pairs further highlights spatial heterogeneity within representative SC-islets. Together, these results demonstrate that impedance spectroscopy enables spatially resolved, cluster-intrinsic interrogation of GSIS, revealing functional heterogeneity within individual SC-islets that is masked by averaged measurements.

4. Conclusion

Reliable functional assessment of insulin secretion remains a central challenge in the development and application of stem cell–derived β-cell products, as conventional GSIS–ELISA assays are limited to end-point, batch-averaged measurements and provide limited insight into secretion dynamics and functional heterogeneity. In this study, we established an impedance spectroscopy based microcavity microelectrode array platform as a label-free, non-invasive, and real-time approach to monitor glucose-stimulated insulin secretion from individual stem cell–derived islet-like clusters. Benchmarking against ELISA measurements and pharmacological inhibition experiments confirmed that impedance spectroscopy derived signal dynamics correlates with secretion-associated functional responses while offering substantially higher temporal resolution than conventional biochemical assays.

Importantly, this platform enables functional interrogation at the level of single clusters and, through advanced microcavity architecture with increased number of microelectrodes, spatially resolved measurements within individual islet-like tissues. These capabilities reveal inter- and intra-cluster functional heterogeneity that is obscured in pooled secretion assays. The qualitative correspondence between spatial impedance profiles and the distribution of insulin-expressing cells supports the physiological relevance of impedance spectroscopy as an indirect readout of β-cell function.

While MEA technologies have been widely applied to planar cell cultures and excitable tissues, their use for impedance-based functional interrogation of three-dimensional islet tissues has not been reported to date. This limits direct comparison with the existing literature but underscores the novelty of the microcavity MEA approach presented here, which enables real-time, label-free functional assessment in a three-dimensional islet context. As an alternative manufacturing strategy, future implementations could employ flexible or conformable electrode architectures to achieve three-dimensional tissue–electrode interfaces, as demonstrated for neural and cardiac organoids.

Although impedance spectroscopy derived signal responses to GSIS revealed high correlation with analysis of biochemical insulin secretion, it is unclear what detailed cellular and molecular mechanism lead to impedance changes and thus, does not replace biochemical assays for absolute quantification of insulin secretion. Furthermore, the chip currently does not support continuously varying glucose stimulation paradigms. Integration of dynamic microfluidic control represents a logical next step to more closely mimic physiological conditions. Beyond SC-islets, the measurement principle is readily applicable to primary human or animal islets and other three-dimensional endocrine microtissues.

Taken together, this work positions impedance spectroscopy on microcavity MEAs as a powerful addition to the functional evaluation toolbox for islet tissues. By enabling real-time, single-cluster and spatially resolved analysis of insulin secretion, this platform provides new opportunities for differentiation protocol optimization, functional drug screening, and the development of advanced potency assays in physiologically relevant three-dimensional human islet models.

CRediT authorship contribution statement

Franziska Dana Zitzmann: Data curation, Methodology, Visualization, Writing – review & editing. **Caroline Remmert:** Data curation, Investigation, Methodology, Visualization, Writing – original draft. **Nicole Katarina Rogers:** Investigation, Methodology, Visualization, Writing – review & editing. **Sabine Schmidt:** Formal analysis, Investigation, Methodology, Writing – review & editing. **Heiko Lickert:** Conceptualization, Funding acquisition, Supervision, Writing – original draft, Writing – review & editing. **Heinz-Georg Jahnke:** Conceptualization, Formal analysis, Funding acquisition, Investigation, Methodology, Visualization, Writing – original draft, Writing – review & editing. **Matthias Meier:** Conceptualization, Data curation, Funding acquisition, Investigation, Project administration, Resources, Supervision, Writing – original draft, Writing – review & editing.

Declaration of competing interest

The authors declare that they have no known competing financial interests or personal relationships that could have appeared to influence the work reported in this paper.

Acknowledgements

This work was supported by the Helmholtz Pioneer Campus and the BMBF (Grant number 013L0251). Franziska Zitzmann was funded by the Federal Ministry for Economics Affairs and Climate Action of Germany (BMWK) (project: “STARK: b-ACTmatter” Grant No. 46SKD023X).

Data availability

Data will be made available on request.

References

Alassaf, A., Ishahak, M., Bowles, A., Agarwal, A., 2020. Microelectrode array based functional testing of pancreatic islet cells. Micromachines 11, 507. https://doi.org/10.3390/mi11050507.

Amin, S., Cook, B., Zhou, T., Ghazizadeh, Z., Lis, R., Zhang, T., Khalaj, M., Crespo, M., Perera, M., Xiang, J.Z., Zhu, Z., Tomishima, M., Liu, C., Naji, A., Evans, T., Huangfu, D., Chen, S., 2018. Discovery of a drug candidate for GLIS3-associated diabetes. Nat. Commun. 9, 2681. https://doi.org/10.1038/s41467-018-04918-x.

Balboa, D., Iworima, D.G., Kieffer, T.J., 2021. Human pluripotent stem cells to model islet defects in diabetes. Front. Endocrinol. 12, 642152. https://doi.org/10.3389/fendo.2021.642152.

Campbell, J.E., Newgard, C.B., 2021. Mechanisms controlling pancreatic islet cell function in insulin secretion. Nat. Rev. Mol. Cell Biol. 22, 142–158. https://doi.org/10.1038/s41580-020-00317-7.

Carlsson, P.-O., Hu, X., Scholz, H., Ingvast, S., Lundgren, T., Scholz, T., Eriksson, O., Liss, P., Yu, D., Deuse, T., Korsgren, O., Schrepfer, S., 2025. Survival of transplanted allogeneic beta cells with no immunosuppression. N. Engl. J. Med. 393, 887–894. https://doi.org/10.1056/nejmoa2503822.

Cuesta-Gomez, N., Verhoeff, K., Jasra, I.T., Pawlick, R., Dadheech, N., Shapiro, A.M.J., 2022. Characterization of stem-cell-derived islets during differentiation and after implantation. Cell Rep. 40, 111238. https://doi.org/10.1016/j.celrep.2022.111238.

Faradji, R.N., Cure, P., Ricordi, C., Alejandro, R., 2019. Islet transplantation and beta cell replacement therapy 161–192. https://doi.org/10.3109/9781420016512-12.

Fleischer, S., Jahnke, H.-G., Fritsche, E., Girard, M., Robitzki, A.A., 2019. Comprehensive human stem cell differentiation in a 2D and 3D mode to cardiomyocytes for long-term cultivation and multiparametric monitoring on a multimodal microelectrode array setup. Biosens. Bioelectron. 126, 624–631. https://doi.org/10.1016/j.bios.2018.10.061.

Genitsaridi, I., Salpea, P., Salim, A., Sajjadi, S.F., Tomic, D., James, S., Thirunavukkarasu, S., Issaka, A., Chen, L., Basit, A., Luk, A.O.Y., Ma, R.C.W., Mbanya, J.C., Ramachandran, A., Wild, S., Duncan, B.B., Boyko, E.J., Magliano, D.J., 2025. Idf Diabetes Atlas: Global, Regional and National Diabetes Prevalence Estimates for 2024 and Projections for 2050. https://doi.org/10.2139/ssrn.5327047.

Gerasimenko, T., Nikulin, S., Zakharova, G., Poloznikov, A., Petrov, V., Baranova, A., Tonevitsky, A., 2020. Impedance spectroscopy as a tool for monitoring performance in 3D models of epithelial tissues. Front. Bioeng. Biotechnol. 7, 474. https://doi.org/10.3389/fbioe.2019.00474.

Glieberman, A.L., Pope, B.D., Melton, D.A., Parker, K.K., 2021. Building biomimetic potency tests for islet transplantation. Diabetes 70, 347–363. https://doi.org/10.2337/db20-0297.

Henquin, J.-C., Dufrane, D., Nenquin, M., 2006. Nutrient control of insulin secretion in isolated normal human islets. Diabetes 55, 3470–3477. https://doi.org/10.2337/db06-0868.

Henriques, F.L., Buckle, I., Forbes, J.M., 2025. Type 1 diabetes mellitus prevention: present and future. Nat. Rev. Endocrinol. 21, 608–622. https://doi.org/10.1038/s41574-025-01128-6.

Hogrebe, N.J., Augsornworawat, P., Maxwell, K.G., Velazco-Cruz, L., Millman, J.R., 2020. Targeting the cytoskeleton to direct pancreatic differentiation of human pluripotent stem cells. Nat. Biotechnol. 38, 460–470. https://doi.org/10.1038/s41587-020-0430-6.

Hu, R., Ma, Q., Kong, Y., Wang, Z., Xu, M., Chen, X., Su, Y., Xiao, T., He, Q., Wang, Xuan, Xu, W., Yang, Y., Wang, Xushu, Li, X., Liu, Y., Chen, S., Zhao, R., Guo, M., Wang, G., Li, W., 2025. A compound screen based on Isogenic hESC-Derived β cell reveals an inhibitor targeting ZnT8-Mediated zinc transportation to protect pancreatic β cell from stress-induced cell death. Adv. Sci. 12, 2413161. https://doi.org/10.1002/advs.202413161.

Jaffredo, M., Krentz, N.A.J., Champon, B., Duff, C.E., Nawaz, S., Beer, N., Honore, C., Clark, A., Rorsman, P., Lang, J., Gloyn, A.L., Raoux, M., Hastoy, B., 2023. Electrophysiological characterisation of iPSC-derived human β-like cells and an SLC30A8 disease model. bioRxiv 10 (17), 561014. https://doi.org/10.1101/2023.10.17.561014, 2023.

Jahnke, H.-G., Poenick, S., Maschke, J., Kendler, M., Simon, J.C., Robitzki, A.A., 2014. Direct chemosensitivity monitoring Ex vivo on undissociated melanoma tumor tissue by impedance spectroscopy. Cancer Res. 74, 6408–6418. https://doi.org/10.1158/0008-5472.can-14-0813.

Kaitsuka, T., 2024. The unique roles of ion channels in pluripotent stem cells in response to biological stimuli. Biology 13, 1043. https://doi.org/10.3390/biology13121043.

Kim, K., Lee, Y., Jung, K.B., Kim, Y., Jang, E., Lee, M., Son, M., Lee, H.J., 2025. Highly stretchable 3D microelectrode array for noninvasive functional evaluation of cardiac spheroids and midbrain organoids. Adv. Mater. 37, e2412953. https://doi.org/10.1002/adma.202412953.

Latres, E., Finan, D.A., Greenstein, J.L., Kowalski, A., Kieffer, T.J., 2019. Navigating two roads to glucose normalization in diabetes: automated insulin delivery devices and cell therapy. Cell Metab. 29, 545–563. https://doi.org/10.1016/j.cmet.2019.02.007.

Lithovius, V., Lahdenpohja, S., Ibrahim, H., Saarimäki-Vire, J., Uusitalo, L., Montaser, H., Mikkola, K., Yim, C.-B., Keller, T., Rajander, J., Balboa, D., Barsby, T., Solin, O., Nuutila, P., Grönroos, T.J., Otonkoski, T., 2024. Non-invasive quantification of stem cell-derived islet graft size and composition. Diabetologia 67, 1912–1929. https://doi.org/10.1007/s00125-024-06194-5.

MacDonald, M.J., Gapinski, J.P., 1989. A rapid ELISA for measuring insulin in a large number of research samples. Metabolism 38, 450–452. https://doi.org/10.1016/0026-0495(89)90197-2.

Mahaddalkar, P.U., Scheibner, K., Pfluger, S., Ansarullah, Sterr, M., Beckenbauer, J., Irmler, M., Beckers, J., Knöbel, S., Lickert, H., 2020. Generation of pancreatic β cells from CD177+ anterior definitive endoderm. Nat. Biotechnol. 38, 1061–1072. https://doi.org/10.1038/s41587-020-0492-5.

Marfil-Garza, B.A., Imes, S., Verhoeff, K., Hefler, J., Lam, A., Dajani, K., Anderson, B., O'Gorman, D., Kin, T., Bigam, D., Senior, P.A., Shapiro, A.M.J., 2022. Pancreatic islet transplantation in type 1 diabetes: 20-year experience from a single-centre cohort in Canada. Lancet Diabetes Endocrinol. 10, 519–532. https://doi.org/10.1016/s2213-8587(22)00114-0.

Mathew-Schmitt, S., Oerter, S., Reitenbach, E., Gätzner, S., Höchner, A., Jahnke, H., Piontek, J., Neuhaus, W., Brachner, A., Metzger, M., Appelt-Menzel, A., 2025. Generation of advanced blood–brain barrier spheroids using human-induced pluripotent stem cell-derived brain capillary endothelial-like cells. Adv. Biol. 9, 2400442. https://doi.org/10.1002/adbi.202400442.

Meyer-Hermann, M.E., 2007. The electrophysiology of the β-Cell based on single transmembrane protein characteristics. Biophys. J. 93, 2952–2968. https://doi.org/10.1529/biophysj.107.106096.

Müller, M., Walkling, J., Seemann, N., Rustenbeck, I., 2023. The dynamics of calcium signaling in beta cells—A discussion on the comparison of experimental and modelling data. Int. J. Mol. Sci. 24, 3206. https://doi.org/10.3390/ijms24043206.

Molano, R.D., Pileggi, A., Tse, H.M., Stabler, C.L., Fraker, C.A., 2024. A static glucose-stimulated insulin secretion (sGSIS) assay that is significantly predictive of time to diabetes reversal in the human islet bioassay. BMJ Open Diab. Res. 12, e003897. https://doi.org/10.1136/bmjdrc-2023-003897. Care.

Pagliuca, F.W., Millman, J.R., Gürtler, M., Segel, M., Dervort, A.V., Ryu, J.H., Peterson, Q.P., Greiner, D., Melton, D.A., 2014. Generation of functional human pancreatic β cells in vitro. Cell 159, 428–439. https://doi.org/10.1016/j.cell.2014.09.040.

Poenick, S., Jahnke, H.-G., Eichler, M., Frost, S., Lilie, H., Robitzki, A.A., 2014. Comparative label-free monitoring of immunotoxin efficacy in 2D and 3D mamma carcinoma in vitro models by impedance spectroscopy. Biosens. Bioelectron. 53, 370–376. https://doi.org/10.1016/j.bios.2013.09.048.

Rosado-Olivieri, E.A., Anderson, K., Kenty, J.H., Melton, D.A., 2019. YAP inhibition enhances the differentiation of functional stem cell-derived insulin-producing β cells. Nat. Commun. 10, 1464. https://doi.org/10.1038/s41467-019-09404-6.

Russell, R., Carnese, P.P., Hennings, T.G., Walker, E.M., Russ, H.A., Liu, J.S., Giacometti, S., Stein, R., Hebrok, M., 2020. Loss of the transcription factor MAFB limits β-cell derivation from human PSCs. Nat. Commun. 11, 2742. https://doi.org/10.1038/s41467-020-16550-9.

Schönecker, S., Kraushaar, U., Düfer, M., Sahr, A., Härdtner, C., Guenther, E., Walther, R., Lendeckel, U., Barthlen, W., Krippeit-Drews, P., Drews, G., 2014. Long-term culture and functionality of pancreatic islets monitored using microelectrode arrays. Integr. Biol. 6, 540–544. https://doi.org/10.1039/c3ib40261d.

Seino, S., Shibasaki, T., Minami, K., 2011. Dynamics of insulin secretion and the clinical implications for obesity and diabetes. J. Clin. Investig. 121, 2118–2125. https://doi.org/10.1172/jci45680.

Shapiro, A.M.J., Pokrywczynska, M., Ricordi, C., 2017. Clinical pancreatic islet transplantation. Nat. Rev. Endocrinol. 13, 268–277. https://doi.org/10.1038/nrendo.2016.178.

Siehler, J., Bilekova, S., Chapouton, P., Dema, A., Albanese, P., Tamara, S., Jain, C., Sterr, M., Enos, S.J., Chen, C., Malhotra, C., Villalba, A., Schomann, L., Bhattacharya, S., Feng, J., Canan, M.A., Ribaudo, F., Ansarullah, Burtscher, I., Ahlbrecht, C., Plettenburg, O., Kurth, T., Scharfmann, R., Speier, S., Scheltema, R.A., Lickert, H., 2024. Inceptor binds to and directs insulin towards lysosomal degradation in β cells. Nat. Metab. 6, 2374–2390. https://doi.org/10.1038/s42255-024-01164-y.

Siehler, J., Blöchinger, A.K., Akgün, M., Wang, X., Shahryari, A., Geerlof, A., Lickert, H., Burtscher, I., 2021a. Generation of a heterozygous C-peptide-mCherry reporter human iPSC line (HMGUi001-A-8). Stem Cell Res. 50, 102126. https://doi.org/10.1016/j.scr.2020.102126.

Siehler, J., Blöchinger, A.K., Meier, M., Lickert, H., 2021b. Engineering islets from stem cells for advanced therapies of diabetes. Nat. Rev. Drug Discov. 20, 920–940. https://doi.org/10.1038/s41573-021-00262-w.

Siehler, J., Blöchinger, A.K., Meier, M., Lickert, H., 2021c. Engineering islets from stem cells for advanced therapies of diabetes. Nat. Rev. Drug Discov. 20, 920–940.

Szabat, M., Modi, H., Ramracheya, R., Girbinger, V., Chan, F., Lee, J.T.C., Piske, M., Kamal, S., Yang, Y.H.C., Welling, A., Rorsman, P., Johnson, J.D., 2015. High-content screening identifies a role for Na+ channels in insulin production. R. Soc. Open Sci. 2, 150306. https://doi.org/10.1098/rsos.150306.

Velazco-Cruz, L., Song, J., Maxwell, K.G., Goedegebuure, M.M., Augsornworawat, P., Hogrebe, N.J., Millman, J.R., 2019. Acquisition of dynamic function in human stem cell-derived β Cecls. Stem Cell Rep. 12, 351–365. https://doi.org/10.1016/j.stemcr.2018.12.012.

Veres, A., Faust, A.L., Bushnell, H.L., Engquist, E.N., Kenty, J.H.-R., Harb, G., Poh, Y.-C., Sintov, E., Gürtler, M., Pagliuca, F.W., Peterson, Q.P., Melton, D.A., 2019a. Charting cellular identity during human in vitro β-cell differentiation. Nature 569, 368–373. https://doi.org/10.1038/s41586-019-1168-5.

Veres, A., Faust, A.L., Bushnell, H.L., Engquist, E.N., Kenty, J.H.-R., Harb, G., Poh, Y.-C., Sintov, E., Gürtler, M., Pagliuca, F.W., Peterson, Q.P., Melton, D.A., 2019b. Charting cellular identity during human in vitro β-cell differentiation. Nature 569, 368–373.

Wang, Shusen, Du, Y., Zhang, B., Meng, G., Liu, Z., Liew, S.Y., Liang, R., Zhang, Z., Cai, X., Wu, S., Gao, W., Zhuang, D., Zou, J., Huang, H., Wang, M., Wang, Xiaofeng, Wang, Xuelian, Liang, T., Liu, T., Gu, J., Liu, N., Wei, Y., Ding, X., Pu, Y., Zhan, Y., Luo, Y., Sun, P., Xie, S., Yang, J., Weng, Y., Zhou, C., Wang, Z., Wang, Shuang, Deng, H., Shen, Z., 2024. Transplantation of chemically induced pluripotent stem-cell-derived islets under abdominal anterior rectus sheath in a type 1 diabetes patient. Cell 187, 6152–6164.e18. https://doi.org/10.1016/j.cell.2024.09.004.

Yang, X., Forró, C., Li, T.L., Miura, Y., Zaluska, T.J., Tsai, C.-T., Kanton, S., McQueen, J. P., Chen, X., Mollo, V., Santoro, F., Pașca, S.P., Cui, B., 2024. Kirigami electronics for long-term electrophysiological recording of human neural organoids and assembloids. Nat. Biotechnol. 42, 1836–1843. https://doi.org/10.1038/s41587-023-02081-3.

Yue, L., Li, J., Yao, M., Song, S., Zhang, X., Wang, Y., 2024. Cutting edge of immune response and immunosuppressants in allogeneic and xenogeneic islet transplantation. Front. Immunol. 15, 1455691. https://doi.org/10.3389/fimmu.2024.1455691.

Zitzmann, F.D., Schmidt, S., Frank, R., Weigel, W., Meier, M., Jahnke, H.-G., 2024. Microcavity well-plate for automated parallel bioelectronic analysis of 3D cell cultures. Biosens. Bioelectron. 250, 116042. https://doi.org/10.1016/j.bios.2024.116042.

Zitzmann, F.D., Schmidt, S., Naumann, M., Belder, D., Jahnke, H.-G., Robitzki, A.A., 2022. Multielectrode biosensor chip for spatial resolution screening of 3D cell models based on microcavity arrays. Biosens. Bioelectron. 202, 114010. https://doi.org/10.1016/j.bios.2022.114010.